Impact of Dust on climate and AMOC during the Last Glacial Maximum Simulated by CESM1.2

Ming Zhang[1], Yonggang Liu[1*], Jiang Zhu[2], Zhuoqun Wang[1], Zhengyu Liu[3]

[1] Laboratory for Climate and Ocean-Atmosphere Studies, Department of Atmospheric and Oceanic Sciences, School of Physics, Peking University, Beijing, 100871, China

[2] Climate and Global Dynamics Laboratory, National Center for Atmospheric Research, Boulder, CO, 80305, USA

[3] Atmospheric Science Program, Department of Geography, Ohio State University, Columbus, Ohio, 43210, USA.

Contact information of the corresponding author

Email: ygliu@pku.edu.cn

Phone: (+86)-10-62768120

Fax: (+86)-10-62751094

Key points:

1) If there were no dust during the Last Glacial Maximum (LGM), global surface temperature would have been lower by 2.4 °C.

2) AMOC would have been 30 % weaker if there were no dust during the LGM.

3) The ocean and sea-ice dynamics amplify the climate impact of dust by a factor of 2.

Abstract

While the impact of dust on climate and Atlantic Meridional Overturning Circulation (AMOC) during the interglacial period such as the mid-Holocene (MH) has been studied extensively, its impact during the glacial period is unclear. Here we investigate how the climate and AMOC would change if there had been no dust during the Last Glacial Maximum (LGM). Model simulations show that the dust removal leads to a global cooling of over 2.4 °C and a weakening of AMOC by ~30 %. Such temperature change is opposite in sign to that for the MH. The cooling is attributed to the increase of snow and ice albedo and weakening of AMOC when dust is removed, and is amplified through a positive feedback between sea ice and AMOC. Our results indicate that the climate and AMOC are more sensitive to dust change during the glacial than the interglacial period.

Plain language summary

Dust in the atmosphere reflects and absorbs sunlight, reducing the shortwave radiation reaching the surface, while the dust deposited on snow and ice reduces the surface albedo and increases the shortwave radiation received at the surface. Our previous work (Zhang et al. 2021) showed dust reduction during the interglacial period (e.g. mid-Holocene; MH) would cause a global warming of 0.1 °C and a weakening of AMOC by 6.2 %. This warming was due to more sunlight received at the surface when atmospheric dust is removed. Here we show that if dust was removed during the Last Glacial Maximum, climate will be cooled significantly rather than warmed. The major reason is that snow on land was much more extensive during LGM than MH, such that the increase of snow albedo after dust removal has a dominating effect on climate. Result suggests that the global climate and AMOC in the glacial period are more sensitive to dust change than those in the interglacial period.

1. Introduction

Dust in the atmosphere reduces the solar insolation received at the surface by reflecting and absorbing sunlight, while dust falling on snow and ice increases the solar insolation received at the surface by reducing the surface albedo. Therefore, variations of surface dust flux and atmospheric dust concentration can affect local and maybe even global climate. On orbital timescales, both dust flux and atmospheric dust concentration fluctuate (Kohfeld and Harrison 2001; Lambert et al. 2008). For example, during the mid-Holocene (MH; 6 ka), dust emission from both North Africa and Arabian Peninsula was much lower than present day (deMenocal et al. 2000; Mashayek and Peltier 2013; McGee et al. 2013; Pausata et al. 2016; Zheng et al. 2013). Such reduction has been shown to affect African monsoon (Pausata et al. 2016; Thompson et al. 2019), tropical cyclone frequency and intensity (Pausata et al. 2017a), El Niño – Southern Oscillation (ENSO; Pausata et al. 2017b), East Asian climate (Huo et al. 2021; Sun et al. 2019) and Atlantic Meridional Overturning Circulation (AMOC; Zhang et al. 2021). Globally, the dust reduction might have induced a global warming of the order 0.1 °C (Liu et al. 2018; Zhang et al. 2021). During the glacial periods, the global dust fluxes are two to five times greater than present day (Kohfeld and Harrison 2001; Maher et al. 2010). However, the role of dust in the global climate and ocean circulation during such periods is still unclear.

The Last Glacial Maximum (LGM; 21 ka) is the nearest glacial period to us, during which the greenhouse gas concentrations (GHGs), glaciers, orbital configuration and thus the climate were different from the present (Braconnot et al. 2007; Kageyama et al. 2017). Proxy reconstructions indicate that the global mean surface temperature (GMST; all temperatures herein are annual mean) during the LGM was 4.4-6.8 ˚C lower than that in the pre-industrial (PI; Tierney et al.

2020). The deep-ocean stratification was strengthened during the LGM, mainly due to the increase of abyssal salinity (Adkins et al. 2002). Accordingly, the North Atlantic Deep Water (NADW) was shallower and the Antarctic Bottom Water (AABW) expanded compared to present-day counterparts (Bohm et al. 2015; Curry and Oppo 2005; Lynch-Stieglitz et al. 2007; Marchitto and Broecker 2006).

The increase of dust emission during the LGM was mainly due to the increase in wind speeds, weakening of the hydrological cycle and expansion in dust source areas (Harrison et al. 2001). Both the observed and simulated results show that atmospheric dust loading during the LGM was 2-3 times of that in present day (Kohfeld and Harrison 2001; Maher et al. 2010; Mahowald et al. 2006b; Werner et al. 2002). The dust deposition rate in polar region even increased by ~20 times (Hansson 1994; Lambert et al. 2008; Mayewski et al. 1994; Petit et al. 1990; Steffensen 1997; Steffensen et al. 2008).

Many studies have investigated the emission and atmospheric loading of dust as well as its influence on radiation, surface temperature and African monsoon etc. during the LGM (Albani and Mahowald 2019; Albani et al. 2014; Mahowald et al. 2006a; Mahowald et al. 2006b; Ohgaito et al. 2018; Sagoo and Storelvmo 2017; Shen et al. 2020). For example, Albani et al. (2014) optimized the dust emission, particle size and optical properties in CAM4 and obtained a dust distribution that best fits reconstructions. They also emphasized the importance of dust' s optical properties and size distribution on the estimation of direct radiative effect and the influence on monsoon (Albani and Mahowald 2019). Dust deposition on snow was able to cause a significant warming (3-5 °C) over Tibet Plateau surface through snow-darkening effect (i.e.

reducing surface albedo by darkening snow and increasing snowmelt; Hansen and Nazarenko 2004; Qian et al. 2014; Shi et al. 2019) during LGM (Shen et al. 2020), showing a much larger influence than in mid-Holocene (Zhang et al. 2021). In the latest Paleoclimate Model Intercomparison Project phase 4 (PMIP4), changes and uncertainties of the dust are also considered in the sensitivity experiments for LGM (Kageyama et al. 2017). However, there has been no attempt to answer the question as to what the climate would have been if there had been no dust during the LGM.

Here we aim to answer this question by modeling the LGM climate both with and without dust. As will be shown later, the impact of dust on LGM climate is much larger than that on the MH climate, and the sign of impact on the GMST is the opposite. We also pay special attention to the impact on AMOC which plays an important role in controlling glacial-interglacial climate shifts by regulating the meridional heat transport and the carbon storage in deep ocean (Brovkin et al. 2007; Denton et al. 2010; Smith and Gent 2010).

2. Model and experiments

2.1 Model description

The fully coupled climate model used here is the Community Earth System Model version 1.2.2 (CESM1.2.2) (http://www2.cesm.ucar.edu/), which reproduces the observed climate features reasonably well among the Coupled Model Intercomparison Project phase 5 (CMIP5) models (Knutti et al. 2013). The atmosphere model, Community Atmosphere Model version 5 (CAM5), represents the aerosol size distribution with a 3-mode Modal Aerosol Model parameterization (CAM5-MAM3) (Neale et al. 2010). The emission, transport and wet and dry deposition of dust

are all treated in the dust module (Ganopolski et al. 2010). In CAM5, only the direct radiative effect of dust is considered (Albani et al. 2014; Neale et al. 2010). The Community Land Model version 4 (CLM4; Lawrence et al. 2011) involves an active carbon-nitrogen (CN) biogeochemical cycle. The snow-darkening effect of dust is considered based on the Snow, Ice and Aerosol Radiation model (SNICAR) (Flanner and Zender 2006; Flanner et al. 2009). The ocean model, Parallel Ocean Program version 2 (POP2; Smith and Gent 2010) uses a new overflow parameterization (OFP; Briegleb et al. 2010) to represent the Nordic Sea overflows (Denmark strait and Faroe Bank Channel) and the Antarctic overflows (Ross Sea and Weddell Sea), which improved the simulations of Gulf Stream path and AMOC (Danabasoglu et al. 2012).

In this study, a horizontal resolution of latitude 1.9°×longitude 2.5° is used for both the atmosphere and land. Both the ocean and sea ice adopt the nominal 1° resolution, which has uniform 1.125° spacing in latitude and uneven spacing in longitude (0.27° near the equator, gradually increasing to the maximum 0.65° at 60° N/S and then decreasing poleward). The north pole of the ocean and sea-ice grids resides in Greenland. In the vertical direction, the atmosphere and ocean grids have 30 and 60 layers, respectively.

2.2 Experiment setup

A summary of the experimental setup is provided in Table S1. One LGM control experiment (called LGMCtl) with an active dust cycle and one sensitivity experiment removing dust (called LGMND) are carried out. The orbital forcing and GHGs in both experiments follow the Paleoclimate Modelling Intercomparison Project phase 3 (PMIP3) protocol. Land ice sheets

(LISs) and the associated changes of sea level and land-sea mask are derived from reconstructed ice-6G model (Peltier et al. 2015). The PI vegetation cover is prescribed in both experiments but the vegetation phenology responds to climate change according to an active CN biogeochemical cycle (Lawrence et al. 2011). In LGMCtl, distribution of surface dust sources is the same as that in PI, neglecting their changes due to glacial dynamics, sea level drop and vegetation changes (Albani et al. 2014; Harrison et al. 2001; Mahowald et al. 2006b). In LGMND, dust is removed by setting the soil erodibility to zero everywhere.

The LGMCtl experiment was integrated for 4000 years. The GMST and the AMOC strength (defined as the maximum Atlantic meridional streamfunction below 500 m depth) still drift at rates of 0.056 °C/1000 year and -0.18 Sv/1000 years, respectively, for the final 1000 years. The LGMND experiment was branched from the year 4001 of LGMCtl and run for 1200 years. The drifts of GMST and AMOC strength are -0.15 °C/1000 years and -2.16 Sv/1000 years, respectively (diagnosed using the final 500 years, Figure S1). As will be seen later, such small drift neither prevents us from understanding the results and mechanism of dust impact nor affects the major conclusions. The final 200 years of data of both experiments are used for analysis.

In order to understand the mechanisms of climate change more clearly, a pair of atmosphere-only experiments, one with dust (LGM_fixedSST) and the other without dust (LGMND_fixedSST), were also carried out in which the sea surface temperature (SST) and sea-ice concentration from LGMCtl are prescribed. The direct impact of dust on climate (i.e. without the feedbacks of ocean and sea ice) can be demonstrated by the results of such experiments. A pair of experiments with slab ocean (LGM_SOM and LGMND_SOM) were also performed to include the feedback from

sea-ice thermodynamics but not the effect of ocean dynamics. To test the influence of the uncertainty in dust emission, we also carried out a pair of prescribed-SST experiments with a different dust source distribution (LGM_fixedSST_gladst and LGMND_fixedSST). More details can be found in Text S1.

3. LGM climatology

The simulated GMST by LGMCtl is 7.66 °C (Table S1), 7.39 °C lower than that in PI (15.05 °C) simulated by the same model with the same resolution. A global surface cooling of 6.8 °C during LGM with CESM1.2.2 was obtained in Zhu and Poulsen (2021) following the PMIP4 protocol (Kageyama et al. 2017), which is within the estimated range of reconstructions (95 % confidence interval: -6.8 ~ -4.4 ˚C; Tierney et al. 2020). The lower LGM temperature here is probably due to two reasons: 1) the vegetation phenology is simulated online, resulting in an increase in surface albedo (Lawrence et al. 2011); 2) the CO_2 concentration used here is slightly lower than that suggested by the PMIP4 protocol (Kageyama et al. 2017). The LGM GMST obtained here is not much colder than the proxy estimates. Compared to PI, cooling occurs all over the world, especially over the elevated continental glaciers and polar oceans where sea ice expands (Figure S2a). Consistent with the surface cooling, the annual-mean precipitation in LGM decreases in most parts of the world, with a global average reduction of 0.49 mm/day (Figure S2b).

The major characteristics of ocean stratification and MOC in LGMCtl agree well with the reconstructions (Adkins et al. 2002; Adkins et al. 2005; Curry and Oppo 2005; Marchitto and Broecker 2006), including saltier and colder water in the deep Southern Ocean (Figures S3a-b), strengthened ocean stratification dominated by salinity change (Figure S3c), a shallower NADW

(Figures S3d-f) and an expanded AABW (Figures S3g-i).

Both total dust emission and atmospheric dust loading simulated by LGMCtl are approximately twice those in PI (6369.17 Tg/year vs 3103.57 Tg/year for dust emission; 41.96 Tg vs 21.83 Tg for dust loading) (Table S1), mainly attributed to the increased wind speeds and weakened hydrological cycle. Distribution of dust emission sources and atmospheric dust loading in LGMCtl are similar to those in PI (Figure S4). The ratio of global dust loading between LGM and PI in our work is within the range from previous studies (Albani and Mahowald 2019; Maher et al. 2010; Takemura et al. 2009; Werner et al. 2002). The possible influence of glaciogenic dust source suggested by Mahowald et al. (2006b) and Albani et al. (2014) is briefly discussed in section 6.

4. Climate and AMOC responses to dust removal

After the dust removal, the simulated LGM GMST decreases by 2.42 °C (Table S1), indicating that dust had a significant warming effect during the LGM. This is opposite to the effect of dust during MH, where dust removal led to a weak global warming (Zhang et al. 2021). The cooling induced by dust removal during the LGM occurs almost everywhere, with the most significant cooling in the high latitudes of both hemispheres (up to 20 °C; Figure 1a) where sea ice expands and thickens (Figure 1g). There is an obvious cooling (~4 °C) over the dust source areas, such as North Africa, Arabian Peninsula, and Central and Western China. Cooling is also seen over the Tibet Plateau, North America and Europe, most likely due to increase in snow depth after the dust removal (Figure 1h, see section 5.2 for more details). Albani and Mahowald (2019) showed that the presence of dust during LGM induced a global warming of 0.15 °C, much weaker than

obtained here. This may be because 1) their simulations were run for only 50 years; 2) the atmospheric module of their model was CAM4, while CAM5 is used herein, both the LGM climatology and its response to dust could be different between the two models. Specifically, the LGM GMST simulated by CAM5 is 2.44 °C lower than that in CAM4 (Kageyama et al. 2021), which may amplify the responses of snow and sea ice in high latitudes after dust removal here.

The annually averaged global-mean precipitation decreases by 0.05 mm/day after dust removal (Table S1). The net precipitation over North Africa is reduced due to the weakened West African summer monsoon; at the same time, anomalous easterly winds bring water vapor to the western North Atlantic, causing an increase in net precipitation there (Figure 1b). This pattern of change in net precipitation is similar to that in MH. The net precipitation also increases over the northern North Atlantic (north of 45° N), but it is mainly due to the decreased local evaporation (not shown).

The AMOC weakens continuously for 700 years after dust is removed (Figure S1b), and becomes 7.71 Sv (-28.7 %) weaker than before dust is removed at the end of simulation (Table S1). Not only weaker, the AMOC is also slightly shallower than before dust is removed (Figure 2a). The maximum March mixed layer depth over Irminger Sea becomes significantly shallower (up to 700 m, Figure 2b), in line with the weakened AMOC. The global northward oceanic heat transport (OHT) across 50° N is reduced by 0.32 petawatt (Figure 2c), also consistent with the weakening of AMOC. The response of AMOC to dust removal is in the same direction as that in MH but has a much larger magnitude, indicating a dependence on background climate state.

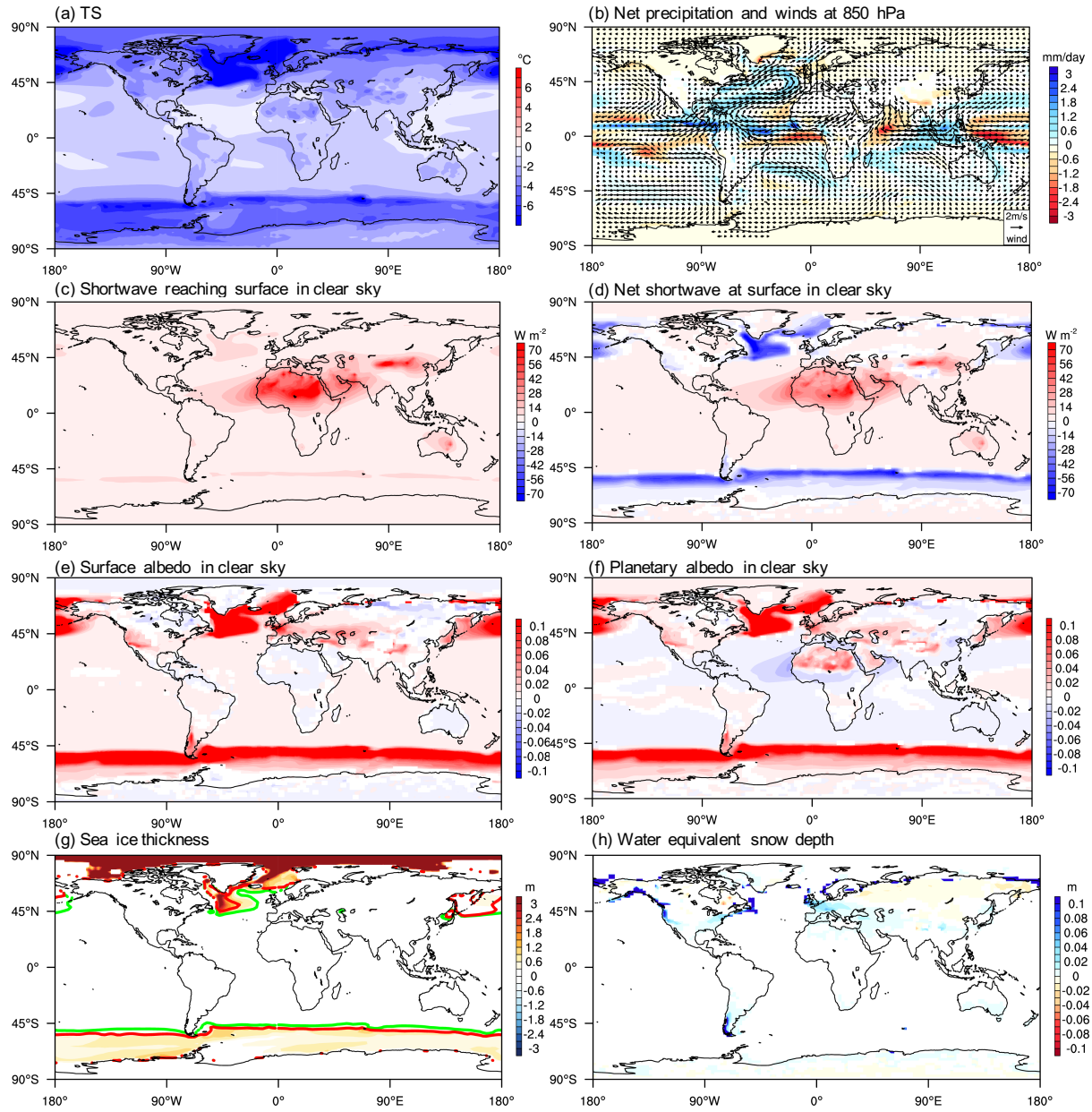

Figure 1. Anomalies of annual mean (a) surface temperature (unit: °C), (b) net precipitation (unit: mm/day) and 850 hPa winds (unit: m/s), (c) downward shortwave radiation at the surface under clear-sky condition (unit: W m^{-2}), (d) net shortwave radiation at the surface under clear-sky condition (unit: W m^{-2}), (e) clear-sky surface albedo, (f) clear-sky planetary albedo, (g) sea-ice thickness (unit: m) and (h) water equivalent snow depth (unit: m) in the LGMND experiment compared to LGMCtl. The green contours and red contours in (g) are the sea-ice margin (defined

as 15 % grid-cell sea-ice coverage) in LGMND and LGMCtl, respectively. Only regions with >90 % confidence level (calculated by two-tailed student-t test) are shown.

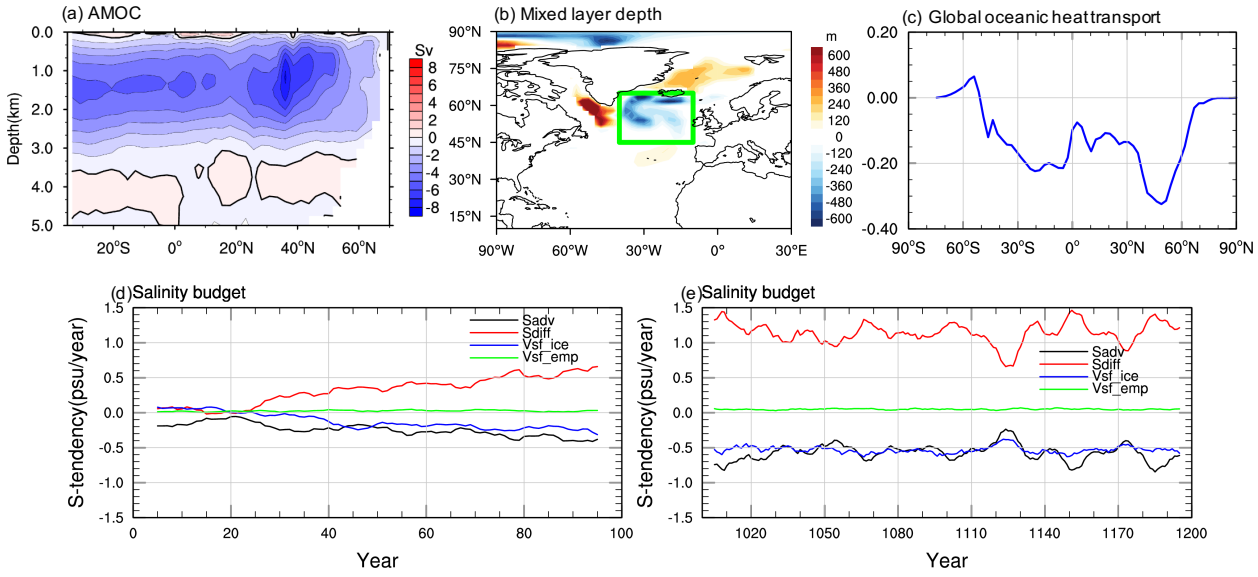

Figure 2. Changes of annual mean Atlantic meridional streamfunction (AMSF, unit: Sv), maximum March mixed layer depth (unit: m) in the Atlantic and global oceanic heat transport (unit: Pw) when dust is removed are shown in a-c and the evolution of anomalies of the terms in the salinity budget equation (Zhang et al. 2021) after dust removal are shown in d-e (unit: psu/year). Zero contour lines are shown in black in (a). The green box (45° N-65° N, 40° W-10° W) in (b) indicates the region where salinity budget is calculated. (d) is for anomalies of the first 100 years and (e) is for anomalies of last 200 years. A moving average of 10 years has been applied to all curves in d-e. The black curve is for horizontal advection (Sadv); red is for diffusion (horizontal plus vertical; Sdiff); blue is for virtual salt flux (VSF) due to sea-ice melting/formation (Vsf_ice); green is for VSF due to net evaporation (Vsf_emp, evaporation minus precipitation minus runoff).

5. Mechanism analyses

5.1 Global surface cooling

The annual-mean shortwave radiation reaching the surface increases (Figure 1c) after dust is removed, especially over regions where atmospheric dust loading was high (Figure S4b). The increased radiation over tropical North Atlantic warms the ocean surface there (Figures 1a, S5a and S5d). However, the net shortwave radiation received by the surface is reduced (Figure 1d) over high latitudes of both hemispheres due to sea ice expansion and thickening (Figure 1g) and over various plateaus (e.g. the Rockies, Iranian and Tibetan Plateau) due to increased snow depth (Figure 1h), all leading to higher surface albedo (Figure 1e). The increase in snow depth is because of the disappearance of snow-darkening effect when there is no dust, while the expansion of sea ice will be analyzed further below. Before that, note that the clear-sky planetary albedo increases over the Sahara and the Arabian region (Figure 1f), where the atmospheric dust loading was the heaviest before being removed (Figure S4b). This means that although this region receives more net shortwave radiation at the surface (Figure 1d), the surface plus the whole atmospheric column actually receives less energy from the Sun when dust is removed. This change of planetary albedo over North Africa and Arabian region is similar to that in Albani et al. (2014) and Albani and Mahowald (2019). The change of global (clearsky) planetary albedo (Figure 1f) indicates that the whole Earth system receives less energy from the Sun and thus should become colder.

The expansion of sea ice plays an important role in both cooling the climate and weakening the AMOC, but it is unclear why sea ice expands in the first place except that the initial AMOC weakening due to dust removal should have some contribution. This initial (first 25 to 50 years)

weakening of AMOC is small (Figure S1b), and is not expected to induce significant sea-ice expansion as can be inferred from the MH results (Zhang et al. 2021). To quantify the contribution of atmospheric and terrestrial components to the global surface cooling after dust removal during LGM, the prescribed-SST experiments are carried out. Result shows that the GMST decreases by 0.31 °C after dust is removed even when SST and sea-ice concentration are fixed (Figure 3a and Table S1). Significant decrease of temperature and increase of albedo occur over some continental regions, especially over high grounds and North Africa and Arabian region (Figures 3a-c), similar to those in the coupled experiments. These changes in temperature and surface albedo over high grounds are due to easier snow accumulation (Figure 3d) after snow-darkening effect is removed. The cooling over land induces global cooling which is amplified over the Arctic region (~3 °C; Figure 3a), which cause more significant sea-ice growth than the initial AMOC weakening as will be confirmed by the result of slab-ocean experiments. The result of prescribed-SST experiments also indicates that the ocean and sea-ice dynamics and the feedback between them have a much stronger cooling effect (2.11 °C) during the LGM than during MH.

The result of the slab-ocean experiments shows that a further global surface cooling of 0.90 °C is obtained when sea ice is allowed to grow (Figure 3e and Table S1). Note that this number may not be so accurate since the slab-ocean experiment (with dust) cannot fully reproduce the surface temperature of the coupled experiment, especially over the Southern Ocean (Figure S6). Interestingly, sea ice within the northern North Atlantic decreases when dust is removed (as can be inferred from the surface albedo change in Figure 3f), demonstrating the importance of ocean dynamics to sea-ice growth in this region. These results imply that the weakening of AMOC and

the associated feedback from sea-ice expansion lead to an additional cooling of roughly 1.21 °C (2.42 °C minus 0.31 minus 0.90 °C).

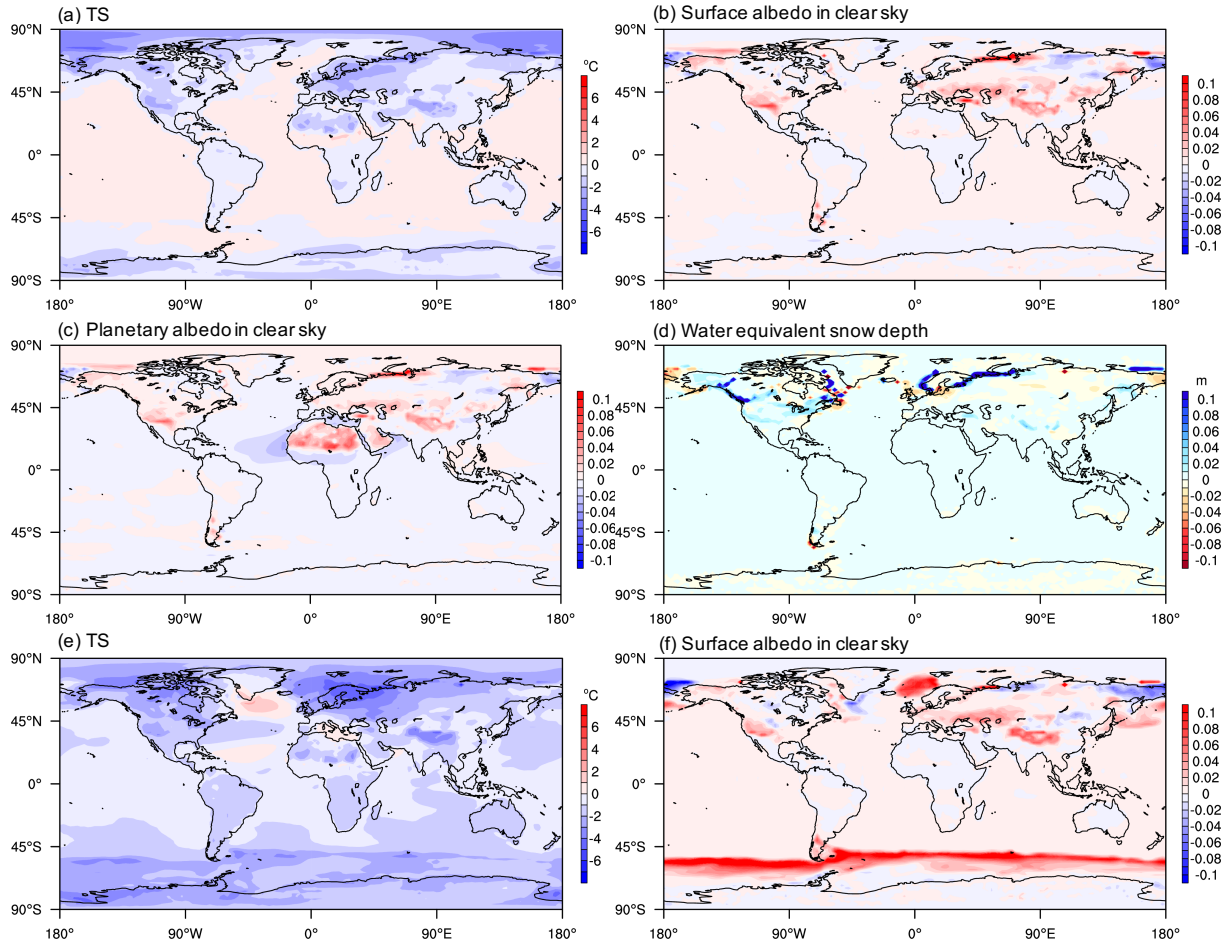

Figure 3. Changes of variables when dust is removed in (a-d) prescribed-SST experiments and (e-f) slab-ocean experiments. All variables are in annual mean, they are: (a) surface temperature (unit: °C), (b) clear-sky surface albedo, (c) planetary albedo in clear sky, (d) water equivalent snow depth (unit: m), (e) clear-sky surface temperature (unit: °C) and (f) surface albedo.

5.2 AMOC change

AMOC weakening is due to the surface density reduction over the northern North Atlantic after

dust removal, while the density reduction itself is due to salinity reduction since temperature change there tends to increase density (Figure S5). Salinity budget for the top 30 m over deep-water formation region near the Irminger Sea (the green box in Figure 2d, 45° N-65° N, 40° W-10° W) is carried out to understand why salinity decreases there. The variation of salinity is decomposed into four components corresponding to four processes: advection, diffusion, sea ice growth and melting, and net evaporation. More details about how they are calculated could be found in Yang and Wen (2020) and Zhang et al. (2021).

Result shows that the evolution of salinity near the Irminger Sea can be divided into two stages, at approximately 25th model year. During the first 25 years, the salinity reduction is solely due to horizontal advection while sea-ice melting becomes more and more important afterwards (Figure 2d). The vertical advection cannot reduce the surface salinity because the salinity is larger at depth than at the surface in that region (not shown). In the last 200 years, the contributions of sea-ice melting and advection to salinity reduction are comparable (~0.6 psu/year). The two terms are balanced mainly by the diffusion term (Figure 2e), while the net evaporation plays a negligible role.

During the first stage, the low-salinity water is advected from the lower latitude to the deepwater formation region, similar to what happens in MH (Zhang et al. 2021). The reduction in dust weakens the monsoonal precipitation over North Africa but strengthens the precipitation in the western North Atlantic (Figure 1b), decreasing the sea surface salinity there (Figure S7a). This salinity anomaly is then advected to the high latitudes by the surface ocean currents (Figures S7a-d), causing the weakening of AMOC.

In the second stage, sea ice in the North Atlantic and Arctic expands and thickens (Figures S7f-h) as a response to the weakening of AMOC and global cooling. This increased sea ice over one of the major deep-water formation regions (green box in Figure 2b) can decrease the surface salinity there directly by melting, as indicated by the blue line in Figure 3. The increased melting of sea ice in the region to the west and south of the deep-water formation region reduces the surface salinity there (Figures S7b-d). This salinity anomaly is also advected to the deep-water formation region by the ocean current, as can be inferred from the concurrent increase of sea-ice and advective contributions to the salinity anomaly since year 25 (Figure 2d). This is the reason why the contribution of advection to salinity anomaly over the deep-water formation region in LGM is significantly greater than that in MH.

Note that most (~80 %) of the sea ice over the northern North Atlantic is not grown in situ, rather it is transported there from the Arctic ocean (not shown). The melting of such sea ice reduces the surface salinity over the northern North Atlantic (45° N-70° N, up to 2.0 psu; Figure S5b). As a result, the salinity induced density stratification over that region strengthens significantly at the end of the simulation (Figure S5).

6. Conclusion and discussion

Opposite to the slight global warming induced by dust removal during MH, a significant cooling of 2.42 °C is obtained for the LGM. However, the AMOC weakens during the LGM when dust is removed, just as in MH, but with a much larger magnitude (-28.7 % vs. -6.2 %). The snow cover and surface albedo increase over high grounds and polar regions due to the removal of

381 snow-darkening effect of the dust. This albedo change induces cooling on land and sea ice, and
382 globally the cooling is 0.31 °C. The thermodynamic sea-ice growth triggered by such cooling
383 induces a further cooling of ~0.90 °C. The rest of the cooling (1.21 °C) is achieved through
384 weakening of AMOC and the positive feedback between sea ice and AMOC. The initial AMOC
385 weakening is due to the advection of negative salinity anomaly to the deep-water formation
386 region from the western North Atlantic. The later weakening is due to increasing sea-ice
387 meltwater within the deep-water formation region both locally and advected from surrounding
388 regions. Our results indicate that the glacial climate and AMOC are much more sensitive to the
389 dust change than their interglacial counterparts; the simulated LGM climate by CESM1.2 would
390 have been much colder if it were not for the existence of dust.
391
392 To test the influence of the uncertainty in dust emission on the results obtained above, we carried
393 out a pair of prescribed-SST experiments with a different dust source distribution. In this
394 distribution, the glaciogenic dust sources (Albani et al. 2014; Mahowald et al. 2006b; Ohgaito et
395 al. 2018) are considered, mainly located in Europe, Siberia, South America and North America
396 (Figure S8a). A total emission of 1090 Tg/year from these additional sources is prescribed
397 according to Albani et al. (2014). Compared to the result in the prescribed-SST LGM experiment
398 described above, the atmospheric dust loading increases near the new dust sources but decreases
399 in Asia, indicating complex interaction between dust and climate (Figure S8c). The total
400 atmospheric dust loading increases slightly by 0.95 Tg and the GMST increases by 0.03 °C
401 (Table S1). This means that removing such dust will induce a cooling of 0.34 °C, only slightly
402 larger than that obtained in section 5.1. The experiments with fully coupled model are therefore
403 not carried out given the expensive computational cost and the likely little gain from the results.

The GMST of MH is similar to that of PI but with warmer polar regions than PI (Braconnot et al. 2007; Brierley et al. 2020; Liu et al. 2018; Zhang et al. 2021). Therefore, the extent of polar sea ice as well as land snow is much smaller than that during the LGM. The removal of dust does not induce significant cooling over land or sea ice, making the surface albedo feedback of sea ice and land snow as well as the interaction between AMOC and sea ice negligible. The result is subject to uncertainties since it is obtained with only a single model. Most other models may obtain smaller climatic impact of dust since their LGM climates are warmer and snow and sea-ice are less than those obtained by CESM1.2.2 (Kageyama et al. 2021).

Acknowledgments

This work is supported by Chinese MOST 2017YFA0603801, NSFC 41888101 and NSFC 41630527. We greatly appreciate the invaluable suggestions from Prof. Samuel Albani at University of Milano-Bicocca and Prof. Zhengguo Shi at Institude of Earth Environment, Chinese Academy of Sciences. Simulations were performed on the Thanhe-2 Supercomputer at the Chinese National Supercomputer Center in Guangzhou and the High-performance Computing Platform of Peking University. The authors declare that they have no competing interests.

Data Availability Statement

Relevant datasets generated in this study are available on Zenodo with the identifier https://zenodo.org/record/5576923#.YW4vNLhByUk.

References

Adkins, J. F., K. McIntyre, and D. P. Schrag, 2002: The salinity, temperature, and delta O-18 of the glacial deep ocean. *Science*, **298,** 1769-1773.

Adkins, J. F., A. P. Ingersoll, and C. Pasquero, 2005: Rapid climate change and conditional instability of the glacial deep ocean from the thermobaric effect and geothermal heating. *Quaternary Sci Rev*, **24,** 581-594.

Albani, S., and N. M. Mahowald, 2019: Paleodust Insights into Dust Impacts on Climate. *J Climate*, **32,** 7897-7913.

Albani, S., and Coauthors, 2014: Improved dust representation in the Community Atmosphere Model. *J Adv Model Earth Sy*, **6,** 541-570.

Bohm, E., and Coauthors, 2015: Strong and deep Atlantic meridional overturning circulation during the last glacial cycle. *Nature*, **517,** 73-U170.

Braconnot, P., and Coauthors, 2007: Results of PMIP2 coupled simulations of the Mid-Holocene and Last Glacial Maximum - Part 1: experiments and large-scale features. *Clim Past*, **3,** 261-277.

Briegleb, B. P., G. Danabasoglu, and W. G. Large, 2010: An overflow parameterization for the ocean component of the Community Climate System Model. *NCAR Tech*, **Note NCAR/ TN-4811STR, 72 pp**.

Brierley, C. M., and Coauthors, 2020: Large-scale features and evaluation of the PMIP4-CMIP6 midHolocene simulations. *Clim Past*, **16,** 1847-1872.

Brovkin, V., A. Ganopolski, D. Archer, and S. Rahmstorf, 2007: Lowering of glacial atmospheric CO2 in response to changes in oceanic circulation and marine biogeochemistry. *Paleoceanography*, **22**.

Curry, W. B., and D. W. Oppo, 2005: Glacial water mass geometry and the distribution of delta

C-13 of Sigma CO2 in the western Atlantic Ocean. *Paleoceanography*, **20**.

Danabasoglu, G., and Coauthors, 2012: The CCSM4 Ocean Component. *J Climate*, **25,** 1361-1389.

deMenocal, P., J. Ortiz, T. Guilderson, J. Adkins, M. Sarnthein, L. Baker, and M. Yarusinsky, 2000: Abrupt onset and termination of the African Humid Period: rapid climate responses to gradual insolation forcing. *Quaternary Sci Rev*, **19,** 347-361.

Denton, G. H., R. F. Anderson, J. R. Toggweiler, R. L. Edwards, J. M. Schaefer, and A. E. Putnam, 2010: The Last Glacial Termination. *Science*, **328,** 1652-1656.

Flanner, M. G., and C. S. Zender, 2006: Linking snowpack microphysics and albedo evolution. *J Geophys Res-Atmos*, **111**.

Flanner, M. G., C. S. Zender, P. G. Hess, N. M. Mahowald, T. H. Painter, V. Ramanathan, and P. J. Rasch, 2009: Springtime warming and reduced snow cover from carbonaceous particles. *Atmos Chem Phys*, **9,** 2481-2497.

Ganopolski, A., R. Calov, and M. Claussen, 2010: Simulation of the last glacial cycle with a coupled climate ice-sheet model of intermediate complexity. *Clim Past*, **6,** 229-244.

Hansen, J., and L. Nazarenko, 2004: Soot climate forcing via snow and ice albedos. *P Natl Acad Sci USA*, **101,** 423-428.

Hansson, M. E., 1994: The Renland Ice Core - a Northern-Hemisphere Record of Aerosol Composition over 120,000 Years. *Tellus B*, **46,** 390-418.

Harrison, S. P., K. E. Kohfeld, C. Roelandt, and T. Claquin, 2001: The role of dust in climate changes today, at the last glacial maximum and in the future. *Earth-Sci Rev*, **54,** 43-80.

Huo, Y., W. R. Peltier, and D. Chandan, 2021: Mid-Holocene monsoons in South and Southeast Asia: dynamically downscaled simulations and the influence of the Green Sahara.

473 Kageyama, M., and Coauthors, 2021: The PMIP4 Last Glacial Maximum experiments:
474 preliminary results and comparison with the PMIP3 simulations. *Clim Past*, **17,** 1065-1089.
475 Kageyama, M., and Coauthors, 2017: The PMIP4 contribution to CMIP6-Part 4: Scientific
476 objectives and experimental design of the PMIP4-CMIP6 Last Glacial Maximum experiments
477 and PMIP4 sensitivity experiments. *Geosci Model Dev*, **10,** 4035-4055.
478 Knutti, R., D. Masson, and A. Gettelman, 2013: Climate model genealogy: Generation CMIP5
479 and how we got there. *Geophys Res Lett*, **40,** 1194-1199.
480 Kohfeld, K. E., and S. P. Harrison, 2001: DIRTMAP: the geological record of dust. *Earth-Sci*
481 *Rev*, **54,** 81-114.
482 Lambert, F., and Coauthors, 2008: Dust-climate couplings over the past 800,000 years from the
483 EPICA Dome C ice core. *Nature*, **452,** 616-619.
484 Lawrence, D. M., and Coauthors, 2011: Parameterization Improvements and Functional and
485 Structural Advances in Version 4 of the Community Land Model. *J Adv Model Earth Sy*, **3**.
486 Liu, Y. G., M. Zhang, Z. Y. Liu, Y. Xia, Y. Huang, Y. R. Peng, and J. Zhu, 2018: A Possible Role
487 of Dust in Resolving the Holocene Temperature Conundrum. *Sci Rep-Uk*, **8**.
488 Lynch-Stieglitz, J., and Coauthors, 2007: Atlantic meridional overturning circulation during the
489 Last Glacial Maximum. *Science*, **316,** 66-69.
490 Maher, B. A., J. M. Prospero, D. Mackie, D. Gaiero, P. P. Hesse, and Y. Balkanski, 2010: Global
491 connections between aeolian dust, climate and ocean biogeochemistry at the present day and at
492 the last glacial maximum. *Earth-Sci Rev*, **99,** 61-97.
493 Mahowald, N. M., M. Yoshioka, W. D. Collins, A. J. Conley, D. W. Fillmore, and D. B. Coleman,
494 2006a: Climate response and radiative forcing from mineral aerosols during the last glacial
495 maximum, pre-industrial, current and doubled-carbon dioxide climates. *Geophys Res Lett*, **33**.

Mahowald, N. M., D. R. Muhs, S. Levis, P. J. Rasch, M. Yoshioka, C. S. Zender, and C. Luo, 2006b: Change in atmospheric mineral aerosols in response to climate: Last glacial period, preindustrial, modern, and doubled carbon dioxide climates. *J Geophys Res-Atmos*, **111**.

Marchitto, T. M., and W. S. Broecker, 2006: Deep water mass geometry in the glacial Atlantic Ocean: A review of constraints from the paleonutrient proxy Cd/Ca. *Geochem Geophy Geosy*, **7**.

Mashayek, A., and W. R. Peltier, 2013: Shear-induced mixing in geophysical flows: does the route to turbulence matter to its efficiency? *J Fluid Mech*, **725,** 216-261.

Mayewski, P. A., and Coauthors, 1994: Changes in Atmospheric Circulation and Ocean Ice Cover over the North-Atlantic during the Last 41,000 Years. *Science*, **263,** 1747-1751.

McGee, D., P. B. deMenocal, G. Winckler, J. B. W. Stuut, and L. I. Bradtmiller, 2013: The magnitude, timing and abruptness of changes in North African dust deposition over the last 20,000 yr. *Earth Planet Sc Lett*, **371,** 163-176.

Neale, R. B., and Coauthors, 2010: Description of the NCAR Community Atmosphere Model (CAM 5.0).

Ohgaito, R., and Coauthors, 2018: Effect of high dust amount on surface temperature during the Last Glacial Maximum: a modelling study using MIROC-ESM. *Clim Past*, **14,** 1565-1581.

Pausata, F. S. R., G. Messori, and Q. Zhang, 2016: Impacts of dust reduction on the northward expansion of the African monsoon during the Green Sahara period. *Earth Planet Sc Lett*, **434,** 298-307.

Pausata, F. S. R., and Coauthors, 2017a: Tropical cyclone activity enhanced by Sahara greening and reduced dust emissions during the African Humid Period. *P Natl Acad Sci USA*, **114,** 6221-6226.

Pausata, F. S. R., and Coauthors, 2017b: Greening of the Sahara suppressed ENSO activity

519 during the mid-Holocene. *Nature Communications*, **8**.
520 Peltier, W. R., D. F. Argus, and R. Drummond, 2015: Space geodesy constrains ice age terminal
521 deglaciation: The global ICE-6G_C (VM5a) model. *J Geophys Res-Sol Ea*, **120,** 450-487.
522 Petit, J. R., L. Mounier, J. Jouzel, Y. S. Korotkevich, V. I. Kotlyakov, and C. Lorius, 1990:
523 Palaeoclimatological and Chronological Implications of the Vostok Core Dust Record. *Nature*,
524 **343,** 56-58.
525 Qian, Y., and Coauthors, 2014: Light-absorbing particles in snow and ice: Measurement and
526 modeling of climatic and hydrological impact. *Adv Atmos Sci*, **32,** 64-91.
527 Sagoo, N., and T. Storelvmo, 2017: Testing the sensitivity of past climates to the indirect effects
528 of dust. *Geophys Res Lett*, **44,** 5807-5817.
529 Shen, J. J., X. N. Xie, X. G. Cheng, and X. D. Liu, 2020: Effects of dust-in-snow forcing over
530 the Tibetan Plateau on the East Asian dust cycle during the Last Glacial Maximum. *Palaeogeogr*
531 *Palaeocl*, **542**.
532 Shi, Z. G., and Coauthors, 2019: Snow-darkening versus direct radiative effects of mineral dust
533 aerosol on the Indian summer monsoon onset: role of temperature change over dust sources.
534 *Atmos Chem Phys*, **19,** 1605-1622.
535 Smith, R. D., and P. Gent, 2010: The Parallel Ocean Program (POP) reference manual, ocean
536 component of the Community Climate System Model (CCSM). *Los Alamos National Laboratory*
537 *Tech. Rep*, **LAUR-10-01853, 141 pp**
538 Steffensen, J. P., 1997: The size distribution of microparticles from selected segments of the
539 Greenland Ice Core Project ice core representing different climatic periods. *J Geophys*
540 *Res-Oceans*, **102,** 26755-26763.
541 Steffensen, J. P., and Coauthors, 2008: High-resolution Greenland Ice Core data show abrupt

542 climate change happens in few years. *Science*, **321,** 680-684.
543 Sun, W. Y., and Coauthors, 2019: Northern Hemisphere Land Monsoon Precipitation Increased
544 by the Green Sahara During Middle Holocene. *Geophys Res Lett*, **46,** 9870-9879.
545 Takemura, T., M. Egashira, K. Matsuzawa, H. Ichijo, R. O'ishi, and A. Abe-Ouchi, 2009: A
546 simulation of the global distribution and radiative forcing of soil dust aerosols at the Last Glacial
547 Maximum. *Atmos Chem Phys*, **9,** 3061-3073.
548 Thompson, A. J., C. B. Skinner, C. J. Poulsen, and J. Zhu, 2019: Modulation of Mid-Holocene
549 African Rainfall by Dust Aerosol Direct and Indirect Effects. *Geophys Res Lett*, **46,** 3917-3926.
550 Tierney, J. E., J. Zhu, J. King, S. B. Malevich, G. J. Hakim, and C. J. Poulsen, 2020: Glacial
551 cooling and climate sensitivity revisited. *Nature*, **584,** 569-+.
552 Werner, M., and Coauthors, 2002: Seasonal and interannual variability of the mineral dust cycle
553 under present and glacial climate conditions. *J Geophys Res-Atmos*, **107**.
554 Yang, H. J., and Q. Wen, 2020: Investigating the Role of the Tibetan Plateau in the Formation of
555 Atlantic Meridional Overturning Circulation. *J Climate*, **33,** 3585-3601.
556 Zhang, M., Y. Liu, J. Zhang, and Q. Wen, 2021: AMOC and Climate Responses to Dust
557 Reduction and Greening of the Sahara during the Mid-Holocene. *J Climate*, **34,** 4893-4912.
558 Zheng, W., B. Wu, J. He, and Y. Yu, 2013: The East Asian Summer Monsoon at mid-Holocene:
559 results from PMIP3 simulations. *Clim Past*, **9,** 453-466.
560 Zhu, J., and C. J. Poulsen, 2021: Last Glacial Maximum (LGM) climate forcing and ocean
561 dynamical feedback and their implications for estimating climate sensitivity. *Clim Past*, **17,**
562 253-267.
563
564